Searching for $t\bar{t}$ resonances at the CERN Large Hadron Collider

U. Baur[*]

Department of Physics, State University of New York, Buffalo, New York 14260, USA

L. H. Orr[+]

Department of Physics and Astronomy, University of Rochester, Rochester, New York 14627, USA
(Received 7 March 2008; published 2 June 2008)

Many new physics models predict resonances with masses in the TeV range which decay into a pair of top quarks. With its large cross section, $t\bar{t}$ production at the Large Hadron Collider (LHC) offers an excellent opportunity to search for such particles. We present a detailed study of the discovery potential of the CERN Large Hadron Collider for Kaluza-Klein (KK) excitations of the gluon in bulk Randall-Sundrum (RS) models in the $t\bar{t} \rightarrow \ell^{\pm}\nu b\bar{b}q\bar{q}'$ ($\ell = e, \mu$) final state. We utilize final states with one or two tagged b-quarks, and two, three or four jets (including b-jets). Our calculations take into account the finite resolution of detectors, the energy loss due to b-quark decays, the expected reduced b-tagging at large $t\bar{t}$ invariant masses, and include the background originating from $Wb\bar{b}$ + jets, $(Wb + W\bar{b})$ + jets, W + jets, and single top + jets production. We derive semirealistic 5σ discovery limits for nine different KK gluon scenarios, and compare them with those for KK gravitons, and a Z_H boson in the Littlest Higgs model. We also analyze the capabilities of the LHC experiments to differentiate between individual KK gluon models and measure the couplings of KK gluons to quarks. We find that, for the parameters and models chosen, KK gluons with masses up to about 4 TeV can be discovered at the LHC. The ability of the LHC to discriminate between different bulk RS models, and to measure the couplings of the KK gluons is found to be highly model dependent.

PACS numbers: 14.65.Ha, 13.85.Qk

I. INTRODUCTION

The first physics run of the Large Hadron Collider (LHC) is scheduled for 2008. Investigating jet, weak boson, and top quark production are the prime goals of the 2008 run. Top pair production at the LHC, with a cross section which is about 2 orders of magnitude larger than at the Fermilab Tevatron, will make it possible to precisely determine the top quark properties [1]. It also offers an excellent opportunity to search for new physics in the early operational phase of the LHC. Once the LHC reaches design luminosity, $t\bar{t}$ production will provide access to new phenomena in the multi-TeV region. Many extensions of the standard model (SM) predict particles which decay into $t\bar{t}$ pairs, and thus show up as resonances in the $t\bar{t}$ invariant mass, $m(t\bar{t})$, distribution. The masses of these particles are typically in the TeV range. For example, topcolor [2,3] and Little Higgs [4–8] models predict weakly coupled new vector bosons, models with extra dimensions [9–11] can have Kaluza-Klein (KK) excitations of the graviton [12,13], the weak [11,14,15], and the strong gauge bosons [16–23] which couple to top quarks, while massive axial vector bosons appear in torsion gravity models [24]. Resonances in the $t\bar{t}$ channel also occur in technicolor [25,26], chiral color [27], and models

with a strong $SU(3) \times SU(3)$ gauge symmetry [28,29]. In some models [12,16–19], the couplings of the new particles to light quarks and gluons is suppressed, and the $t\bar{t}$ final state becomes their main discovery channel. For a model independent approach to search for new physics in $t\bar{t}$ production, see Ref. [30].

Top quarks decay either hadronically, $t \rightarrow Wb \rightarrow bq\bar{q}'$ ($q, q' = u, d, s, c$), or semileptonically, $t \rightarrow Wb \rightarrow b\ell\nu$ ($\ell = e, \mu$; decays with τ leptons in the final state are ignored here). Pair production of top quarks thus results in so-called " dilepton + jets" events, $t\bar{t} \rightarrow \ell^{\pm}\nu_{\ell}\ell'^{\mp}\nu_{\ell'}b\bar{b}$, " lepton + jets" events, $t\bar{t} \rightarrow \ell^{\pm}\nu b\bar{b}q\bar{q}'$, or the "all-hadronic," $t\bar{t} \rightarrow b\bar{b} + 4$ quarks, final state. Although the dilepton + jets channel has the smallest background, it suffers from a small branching ratio (about 4.7%). Furthermore, the two neutrinos in the final state make it impossible to reconstruct the $t\bar{t}$ invariant mass or the transverse momentum (p_T) of the individual top quark. The all-hadronic final state has the largest branching ratio ($\approx 46\%$) but also suffers from a very large background. The lepton + jets channel, finally, has a substantial branching fraction (about 30%), while the background is moderate. Since the $t\bar{t}$ invariant mass can be reconstructed, albeit with a two-fold ambiguity, it is the premier search channel for new physics in $t\bar{t}$ production. To identify $t\bar{t}$ lepton + jets events, the LHC experiments require an isolated charged lepton, missing transverse momentum, and at least four isolated hadronic jets. For events with more than four

*baur@ubhex.physics.buffalo.edu
+orr@pas.rochester.edu

jets, the four leading (highest transverse momentum) jets are selected. Of these four jets two have to be tagged as a b quarks [31,32].

Searching for $t\bar{t}$ resonances with masses in the TeV region is challenging for several reasons. For top quark transverse momenta larger than a few hundred GeV and $t\bar{t}$ invariant masses above 1 TeV, the top quark decay products are highly boosted and thus almost collinear. This frequently results in nonisolated leptons and/or merged or overlapping jets for lepton + jets and all-hadronic $t\bar{t}$ events, i.e. the number of jets may be smaller than the number of final state quarks. Furthermore, the b-tagging efficiency in the TeV region may be significantly smaller than at low energies [8,17,22].

Extending the selection criteria to include topologies with fewer jets and events with only one tagged b quark is an obvious strategy for improving the selection efficiency for very energetic top quarks. On the other hand, this may significantly increase the background. In Ref. [33] we presented a detailed analysis of the $t\bar{t}$ lepton + jets finals states with 2, 3, or 4 jets and one or two tagged b quarks. We showed that the $\ell\nu + 2$ jets and $\ell\nu + 3$ jets final states with one or two b tags significantly improve the chances for discovering new heavy particles in the $t\bar{t}$ channel at the LHC, although the background from W + jets and single top production will be non-negligible in the TeV region, even after imposing suitable cuts.

In this paper, we derive semirealistic discovery limits for $t\bar{t}$ resonances in the lepton + jets final states using the results of Ref. [33]. We consider Kaluza-Klein excitations of the gluon in representative bulk Randall-Sundrum (RS) models, in particular, those described in Refs. [18,19]. Taking into account the finite resolution of the LHC detectors, the energy loss due to b-quark decays, the expected reduced b-tagging efficiency at large $t\bar{t}$ invariant masses, and the background originating from $Wb\bar{b}$ + jets, $(Wb + W\bar{b})$ + jets, W + jets, and single top + jets production, we derive 5σ discovery limits and contrast them with those found for KK gravitons in bulk RS models [12] and the Z_H boson of the Littlest Higgs model [6]. We also study how

well the KK gluons of various bulk RS models can be discriminated and how well their couplings can be determined at the LHC. In Sec. II we present a brief overview of the couplings of the KK gluons we consider and give an outline of our calculation. Numerical results are presented in Sec. III. Section IV contains our conclusions.

II. KALUZA-KLEIN GLUONS: SIGNAL AND BACKGROUND

We concentrate on the search for the first excited state of the gluon, G, in variants of the RS model with the SM fields propagating in the bulk. Such models can incorporate grand unification of couplings [34], motivate the flavor hierarchy of fermion masses [35], and incorporate a dark matter candidate [36]. Bulk RS models with large brane kinetic terms [37] or an expanded custodial symmetry [16,38,39] may be able to protect the $Zb\bar{b}$ vertex from large corrections [38–41]. Specifically, we consider the KK gluons of the models of Ref. [19] (E_i, $i = 1, \ldots, 4$), the basic RS model with the SM in the bulk [17], models with large brane kinetic terms with magnitude $\kappa r_{IR} = 5$ and $\kappa r_{IR} = 20$, and a model with a $SO(5) \times U(1)_X$ bulk gauge symmetry [41].

The KK gluons of all models considered here couple uniformly to left-handed and right-handed light quarks $q = u, d, s, c$. The couplings and branching ratios to light, bottom, and top quarks, g^q, $g_L^b = g_L^t$, g_R^b, and g_R^t, and the total width, Γ_G, in units of the KK gluon mass, M_G, are listed in Table I. They agree with the results given in Refs. [18,19]. Note that KK gluons do *not* couple vector-like to the quarks of the third generation. The partial width for the decay of a KK gluon into a quark-antiquark pair, $q\bar{q}$, in the limit $M_G \gg m_q$, is given by

$$\Gamma(G \rightarrow q\bar{q}) = \frac{M_G}{48\pi}(g_L^2 + g_R^2), \qquad (1)$$

where g_L (g_R) is the coupling of the left-handed (right-handed) quark to the KK gluon. At tree level, KK gluons do not couple to regular gluons. With the exception of models with a large brane kinetic term, the couplings of KK gluons

TABLE I. The couplings, branching ratios, and the total width in units of the mass, Γ_G/M_G, of KK gluons in various bulk RS models. g_s is the strong coupling constant. In order to calculate Γ_G we have assumed that $\alpha_s = g_s^2/4\pi = 0.1$. N is the number of the additional KK custodial partner quarks in the $SO(5)$ model which are light enough that G can decay into them.

Model	g^q	$g_L^b = g_L^t$	g_R^b	g_R^t	$\sum_q BR(G \rightarrow q\bar{q})$	$BR(G \rightarrow b\bar{b})$	$BR(G \rightarrow t\bar{t})$	Γ_G/M_G
Basic RS	$-0.2g_s$	g_s	$-0.2g_s$	$4g_s$	1.7%	5.7%	92.6%	0.153
$\kappa r_{IR} = 5$	$-0.4g_s$	$-0.2g_s$	$-0.4g_s$	$0.6g_s$	68.1%	10.6%	21.3%	0.016
$\kappa r_{IR} = 20$	$-0.8g_s$	$-0.6g_s$	$-0.8g_s$	$-0.2g_s$	78.5%	15.3%	6.1%	0.054
$SO(5), \ N = 0$	$-0.2g_s$	$2.76g_s$	$-0.2g_s$	$0.07g_s$	2.0%	49.1%	48.9%	0.130
$SO(5), \ N = 1$	$-0.2g_s$	$2.76g_s$	$-0.2g_s$	$0.07g_s$	0.7%	16.0%	15.9%	0.400
E_1	$-0.2g_s$	$1.34g_s$	$0.55g_s$	$4.9g_s$	1.1%	7.4%	91.4%	0.235
E_2	$-0.2g_s$	$1.34g_s$	$3.04g_s$	$4.9g_s$	0.9%	29.7%	69.4%	0.310
E_3	$-0.2g_s$	$1.34g_s$	$0.55g_s$	$3.25g_s$	2.2%	14.2%	83.6%	0.123
E_4	$-0.2g_s$	$1.34g_s$	$3.04g_s$	$3.25g_s$	1.3%	46.6%	52.1%	0.198

to light quarks is suppressed, whereas those to top quarks are enhanced. In these models, $t\bar{t}$ production offers the best chance to discover KK gluons. In models with a large brane kinetic term, KK gluons may also be visible in dijet production [18]. In all models, except those with a large brane kinetic term, the KK gluons are fairly broad resonances.

All cross sections in this paper are computed using CTEQ6L1 [42] parton distribution functions (PDFs). For the CTEQ6L1 PDFs, the strong coupling constant is evaluated at leading order with $\alpha_s(M_Z^2) = 0.130$. The factorization and renormalization scales for the calculation of the $t\bar{t}$ signal are set equal to $\sqrt{m_t^2 + p_T^2(t)}$, where $m_t = 173$ GeV is the top quark mass. The value of the top quark mass chosen is consistent with the most recent experimental data [43]. The choice of factorization and renormalization scales of the background processes is discussed in more detail below. The SM parameters used in all tree-level calculations are [44]

$$G_\mu = 1.16639 \times 10^{-5} \text{ GeV}^{-2}, \tag{2}$$

$$M_Z = 91.188 \text{ GeV}, \qquad M_W = 80.419 \text{ GeV}, \tag{3}$$

$$\sin^2\theta_W = 1 - \left(\frac{M_W^2}{M_Z^2}\right), \qquad \alpha_{G_\mu} = \frac{\sqrt{2}}{\pi} G_F \sin^2\theta_W M_W^2, \tag{4}$$

where G_F is the Fermi constant, M_W and M_Z are the W and Z boson masses, θ_W is the weak mixing angle, and α_{G_μ} is the electromagnetic coupling constant in the G_μ scheme.

We calculate the $t\bar{t} \to \ell\nu b\bar{b}q\bar{q}'$ cross section at leading order (LO), including the contributions from KK gluons and all decay correlations, using the helicity spinor technique described in Ref. [45]. Top quark and W decays are treated in the narrow width approximation. We require that at least one b quark be tagged and that there are a total of two, three, or four jets in the event. We sum over electron and muon final states and impose the following acceptance cuts on lepton + jets events at the LHC (pp collisions at $\sqrt{s} = 14$ TeV)

$$p_T(\ell) > 20 \text{ GeV}, \qquad |\eta(\ell)| < 2.5, \tag{5}$$

$$p_T(j) > 30 \text{ GeV}, \qquad |\eta(j)| < 2.5, \tag{6}$$

$$p_T(b) > 30 \text{ GeV}, \qquad |y(b)| < 2.5, \tag{7}$$

$$\not{p}_T > 40 \text{ GeV}. \tag{8}$$

Here, η (y) is the pseudorapidity (rapidity), $\ell = e, \mu$, and $\not{p}_T$ is the missing transverse momentum originating from the neutrino in $t \to b\ell\nu$ which escapes undetected. In addition, we impose an isolation cut on the charged lepton and jets by requiring the separation in pseudorapidity— azimuth space to be larger than

$$\Delta R = [(\Delta\eta)^2 + (\Delta\Phi)^2]^{1/2} > 0.4. \tag{9}$$

Light quark jets from $W \to q\bar{q}'$ and b-quark jets are merged if

$$\Delta R(i, j) < 0.4, \tag{10}$$

$i, j = q, q', b$. If a b-quark jet and a light quark jet merge, their momenta are combined into a b jet.

The cuts listed in Eqs. (5)–(8) are sufficient for the LHC operating at low luminosity, $\mathcal{L} \leq 10^{33}$ cm^{-2} s^{-1}. They should be tightened somewhat for luminosities closer to the design luminosity, $\mathcal{L} = 10^{34}$ cm^{-2} s^{-1}. However, this will have only a small effect on the cross section in the TeV region on which we concentrate in this paper.

We include minimal detector effects via Gaussian smearing of parton momenta according to ATLAS [31] expectations, and take into account the b-jet energy loss via a parametrized function (for details see Ref. [33]). Charged leptons are assumed to be detected with an efficiency of $\epsilon_\ell = 0.85$.

At low energies, the LHC experiments are expected to tag b jets with an efficiency of $\epsilon_b \approx 0.6$ [31,32]. However, for very energetic top quarks, the b-tagging efficiency is expected to degrade [17]. As we shall see in Sec. III, the range of $m(t\bar{t}) = 2.5$–4.0 TeV will be of interest for KK gluon searches at the LHC. Preliminary ATLAS studies find that, in this region, ϵ_b is about a factor 3 smaller than at low energies [8,22]. For realistic cross section estimates, a parametrization of ϵ_b as a function of the b-quark energy or p_T is needed. Currently, these do not exist. Except for low energies, ϵ_b is known only for a few selected values of $m(t\bar{t})$ [8,22]. In the following, we therefore assume a constant b-tagging efficiency of $\epsilon_b = 0.2$. Note that, for $\epsilon_b = 0.2$, the cross section for final states with one b tag is almost 1 order of magnitude larger than that for two tagged b quarks.

New particles which decay into a pair of top quarks lead to resonances in the $t\bar{t}$ invariant mass distribution and to a Jacobian peak in the top quark transverse momentum distribution. In the following, we therefore concentrate on these observables. The coupling of KK gluons to the top quark is reflected also in the p_T distribution of the charged lepton, which acts as an analyzer of the top polarization [17]. We do not study the $p_T(\ell)$ distribution here.

Since the neutrino escapes undetected, $m(t\bar{t})$ cannot be directly reconstructed. However, assuming that the charged lepton and the missing transverse momentum come from a W boson with a fixed invariant mass $m(\ell\nu) = M_W$, it is possible to reconstruct the longitudinal momentum of the neutrino, $p_L(\nu)$, albeit with a twofold ambiguity. In our calculations of the $m(t\bar{t})$ distribution in the lepton + jets final state, we reconstruct the $t\bar{t}$ invariant mass using both solutions for $p_L(\nu)$ with equal weight. Jets are counted and used in the reconstruction of $m(t\bar{t})$ if they satisfy Eqs. (6) and (7) after merging. The energy loss of the b quarks slightly distorts the $\not{p}_T$ distribution. As a result, the qua-

dratic equation for $p_L(\nu)$ does not always have a solution. Events for which this is the case are discarded in our analysis. This results in a $\approx 10\%$ reduction of the $t\bar{t}$ cross section in the $m(t\bar{t})$ distribution. More advanced algorithms [46] improve the reconstruction of the mass of the new physics signal; however, they have little effect on the shape of the SM $m(t\bar{t})$ distribution. For the background processes, the $m(t\bar{t})$ distribution is replaced by the reconstructed $Wb\bar{b} + m$ jets and $Wbj + m$ jets invariant mass distribution.

In order to reconstruct the t or $\bar{t}$ transverse momentum, one has to correctly assign the b and $\bar{b}$ momenta to the parent top or antitop quark. Since it is impossible to determine the b charge on an event-by-event basis, and we do only require one b tag in the event, we combine $\not{p}_T$, $p_T(\ell)$, and the transverse momentum of the jet with the smallest separation from the charged lepton to form the transverse momentum of the semileptonically decaying top quark. The p_T's of the remaining jet(s) form the transverse momentum of the hadronically decaying top.[1] We find that the reconstructed and true top quark transverse momentum distributions are virtually identical except for transverse momenta below 50 GeV where deviations at the few percent level are observed.

The main background processes contributing to the $\ell\nu + n$ jet final states with $n = 2, 3, 4$ are $Wb\bar{b} + m$ jets, $(Wb + W\bar{b})j + m$ jets, and $Wjj + m$ jets production, $(t\bar{b} + \bar{t}b) + m$ jets, $(t + \bar{t})j + m$ jets production with $t \rightarrow b\ell\nu$, and Wbt, Wt, and Wjt production with $t \rightarrow bjj$. For each process, $m = 0, 1, 2$, and j represents a light quark or gluon jet, or a c jet. Wt production only contributes to the two jet and three jet final states. The $(Wb + W\bar{b})j + m$ jets $((t + \bar{t})j + m$ jets) background originates from $Wb\bar{b}j + m$ jets $((t\bar{b} + \bar{t}b) + m$ jets) production where one of the b quarks is not detected. We calculate these processes in the b-quark structure function approximation. We have verified that, for $m = 0$, the differential cross sections for $pp \rightarrow Wbj$ $((t + \bar{t})j)$ and $pp \rightarrow Wb\bar{b}j$ $((t\bar{b} + \bar{t}b)j)$ where one b jet is not detected are very similar. All background cross sections are consistently calculated at LO. To calculate $pp \rightarrow Wb\bar{b} + m$ jets and $pp \rightarrow Wjj + m$ jets we use ALPGEN [44]. All other background processes are calculated using MADEVENT [48].

Background processes, such as $pp \rightarrow Wjj + m$ jets, where one or two jets are misidentified as b jets are calculated using a misidentification probability of $P_{q,g \rightarrow b} = P_{j \rightarrow b} = 1/30$ ($q = u, d, s$) for light jets, and $P_{c \rightarrow b} = 1/10$ for charm quarks. Preliminary ATLAS studies [8,22] have found these values to be appropriate in the $t\bar{t}$ invariant mass region around 3 TeV which is the range on which this paper concentrates. Ideally, one would like to know $P_{j \rightarrow b}$ and $P_{c \rightarrow b}$ as functions of the jet transverse

momentum. Unfortunately, these parametrizations are presently not available.

$Wjj + m$ jets production in ALPGEN includes c jets in the final state. Since $P_{c \rightarrow b}$ is considerably larger than $P_{q,g \rightarrow b}$, this underestimates the background from $W +$ charm production. However, the cross section of $W +$ charm final states is only a tiny fraction of the full $Wjj + m$ jets rate, resulting in an error which is much smaller than the uncertainty on the background from other sources. One can also estimate the $W +$ charm cross section from that of $pp \rightarrow Wb\bar{b} + m$ jets and $pp \rightarrow (Wb + W\bar{b}) + m$ jets. For the phase space cuts imposed, quark mass effects are irrelevant. Using the values of $P_{c \rightarrow b}$ given in Refs. [8,22,31], we find that the $(Wc + W\bar{c})j + m$ jets $(Wc\bar{c} + m$ jets) cross section is a factor 2–10 (5–100) smaller than the $(Wb + W\bar{b})j + m$ jets $(Wb\bar{b} + m$ jets) rate for the p_T and invariant mass range considered here.

$b\bar{b} + m$ jets production where one b quark decays semileptonically also contributes to the background. Once a lepton isolation cut has been imposed, this background is known to be small for standard lepton + jets cuts [49]. For $b\bar{b} + m$ jets events to mimic $t\bar{t}$ production with very energetic top quarks, the b quarks also have to be very energetic. This will make the lepton isolation cut even more efficient. We therefore ignore the $b\bar{b} + m$ jets background here.

The renormalization and factorization scales, μ_r and μ_f, of background processes involving top quarks are set to m_t; for all other background processes we choose the W mass. Since our calculations are performed at tree level, the cross section of many background processes exhibits a considerable scale dependence. However, uncertainties on the current b-tagging efficiencies and the light jet mistag probability at high energies introduce an uncertainty which may well be larger. Our choice of μ_r and μ_f leads to a rather conservative estimate of the background cross sections; other (reasonable) choices such as $\mu_r^2 = \mu_f^2 = M_W^2 + \sum_i p_T(j_i)^2$, where i runs over all jets, lead to smaller cross sections, especially at high energies.

Without further cuts, the background turns out to be much larger than the signal for $t\bar{t}$ invariant masses in the TeV region [33]. The signal to background ratio, however, can be improved significantly by imposing a cut

$$|m_T(j_{\min}\ell) - m_t| < 20 \text{ GeV} \qquad (11)$$

on the cluster transverse mass, m_T, and a cut

$$|m(t \rightarrow nj) - m_t| < 20 \text{ GeV}, \qquad (12)$$

on invariant mass of the $n = 1, 2$ or 3 remaining jets which are assumed to originate from the hadronically decaying top quark. The cluster transverse mass in Eq. (11) is defined by

---

[1]Alternatively, one could select the combination of jets which minimizes $|m(jets) - m_t|$ [47].

$$m_T^2(j_{\min}\ell) = (\sqrt{p_T^2(j_{\min}\ell) + m^2(j_{\min}\ell)} + \not{p}_T)^2$$
$$- (\vec{p}_T(j_{\min}\ell) + \vec{\not{p}}_T)^2, \qquad (13)$$

where $p_T(j_{\min}\ell)$ and $m(j_{\min}\ell)$ are the transverse momentum and invariant mass of the $j_{\min}\ell$ system, respectively, and $j_{\min}$ is the jet with the smallest separation from the charged lepton. m_T sharply peaks at the top mass. The invariant mass resolution for jet systems with a mass near m_t is approximately 7–10 GeV for jets with energies above 200 GeV. The invariant mass window chosen in Eq. (12) thus will capture most of the $t\bar{t}$ signal. On the other hand, it is sufficiently narrow to reject a large portion of the background.

In case of only two jets in the final state, we impose Eq. (12) on the jet with the larger separation from the charged lepton. In order to estimate the effect of a jet invariant mass cut on the Wjj and $(t + \bar{t})j$ background, we convolute the differential cross sections obtained from ALPGEN and MADEVENT with $\mathcal{P}(m(j_{\text{top}}), p_T(j_{\text{top}}))$ where j_{top} is the jet with the larger separation from the charged lepton (i.e. the "t-jet" candidate) [33]. A cut on $m(j_{\text{top}})$ is then imposed (see below). $\mathcal{P}(m(j), p_T(j))$ is the two-dimensional probability density that a jet with transverse momentum $p_T(j)$ has an invariant mass $m(j)$. We calculate $\mathcal{P}(m(j), p_T(j))$ by generating 10^5 $W + \text{jets}$ events in PYTHIA [50] and passing them through PGS4 [51], which simulates the response of a generic high-energy physics collider detector with a tracking system, electromagnetic and hadronic calorimetry, and muon system. Jets are reconstructed in the cone [52] and k_T algorithms [53] as implemented in PGS4, using a cone size (D parameter) of $R = 0.5$ ($D = 0.5$) in the cone (k_T) algorithm. Since it is infrared safe, the k_T algorithm is the theoretically preferred algorithm. For a discussion of the advantages and disadvantages of the two algorithms at hadron colliders, see Ref. [54]. The cone size (D parameter) is deliberately chosen to be slightly larger than in our parton level studies to avoid drawing conclusions which are too optimistic. The probability density function, $\mathcal{P}$, for the k_T algorithm has a much longer tail at large jet invariant masses than for the cone algorithm, resulting in a significantly higher background in the $m(t\bar{t})$ distribution [33]. In order to be conservative, we therefore use the k_T algorithm when estimating the background in the $\ell\nu + 2\,\text{jets}$ final state.

The reconstructed $m(t\bar{t})$ distribution after imposing the cuts listed in Eqs. (5)–(12) is shown in Fig. 1 for the range $|M_G - m(t\bar{t})| \leq 1$ TeV. We show the results for the combined $t\bar{t} \rightarrow \ell\nu + n\,\text{jets}$ final states with $n = 2, 3, 4$, and one or two tagged b quarks, assuming $\epsilon_b = 0.2$ and $\epsilon_\ell = 0.85$. The curves are for SM $t\bar{t}$ production (solid black line), the combined background (blue histogram), and KK gluon production with $M_G = 3$ TeV for the models listed in Table I. The transverse momentum distribution of the semileptonically decaying top quark is shown in Fig. 2.
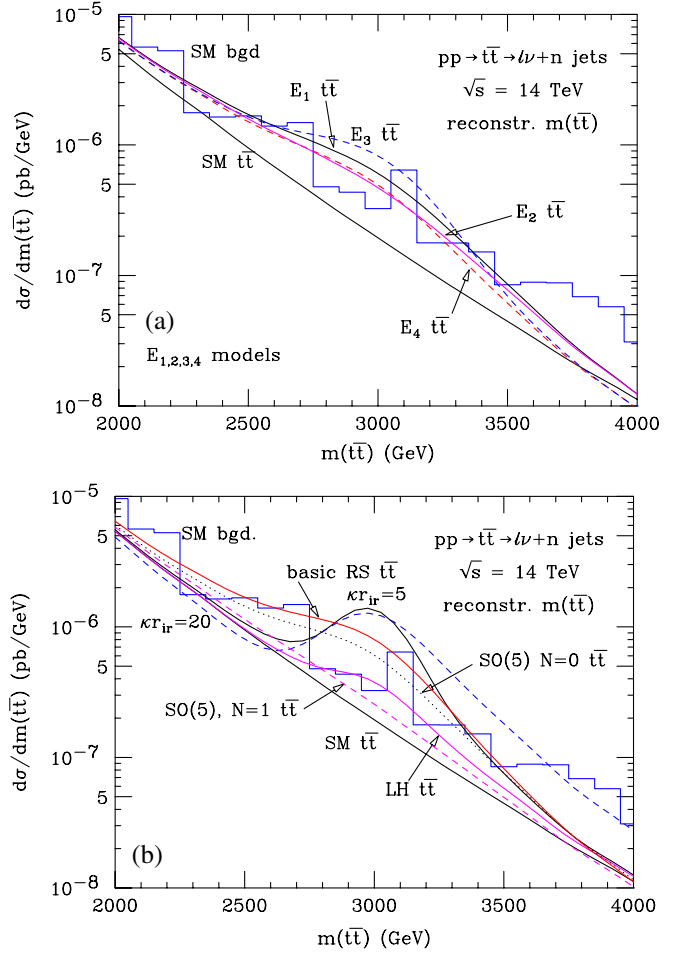
FIG. 1 (color online). The LO differential cross section of the combined SM $t\bar{t} \rightarrow \ell\nu + n\,\text{jets}$ ($n = 2, 3, 4$) signal (black line), the combined background (blue histogram), and a bulk RS KK gluon, G, with $M_G = 3$ TeV as a function of the reconstructed $t\bar{t}$ invariant mass. One or two of the jets are assumed to be b tagged. Part (a) of the figure shows the results for E_i ($i = 1, \ldots, 4$) KK gluons, part (b) shows the resonance curves for the remaining KK gluon scenarios summarized in Table I. For comparison, the magenta line in (b) shows the result for a Z_H boson in the Littlest Higgs model with a mass of 3 TeV and $\cot\theta = 1$ (see Ref. [6]). The cuts imposed are discussed in the text.

To avoid overburdening the figures, we show the E_i ($i = 1, \ldots, 4$) KK gluon resonances in Figs. 1(a) and 2(a), and all others in Figs. 1(b) and 2(b), respectively. For comparison, the magenta line in Figs. 1(b) and 2(b) shows the result for a Z_H boson in the Littlest Higgs model with $M_{Z_H} = 3$ TeV and $\cot\theta = 1$ (see Ref. [6]), where θ is a mixing angle. The Z_H vector boson couples purely left-handed and universally to quarks and leptons.

For all models, except that with $\kappa r_{IR} = 20$, the sign of the coupling of the KK gluon to light quarks is opposite to that of the larger coupling to the top quark. As a result, in those cases, interference effects are positive (negative)
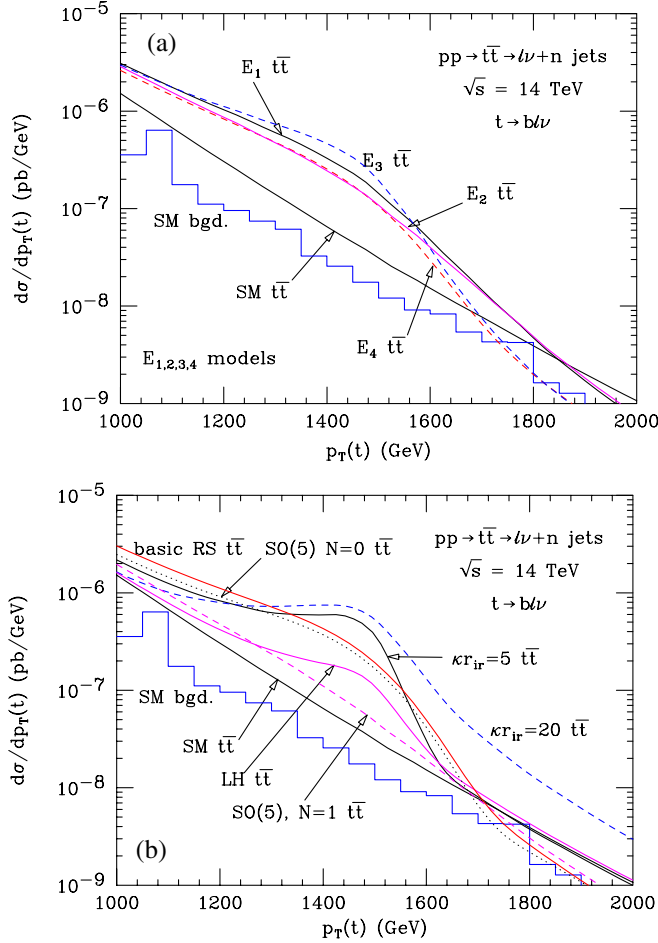
FIG. 2 (color online).   The LO differential cross section of the combined SM $t\bar{t} \to \ell\nu + n$ jets ($n = 2, 3, 4$) signal (black line), the combined background (blue histogram), and a bulk RS KK gluon, G, with $M_G = 3$ TeV as a function of the reconstructed transverse momentum of the semileptonically decaying top quark. One or two of the jets are assumed to be b tagged. Part (a) of the figure shows the results for E_i ($i = 1, \ldots, 4$) KK gluons, part (b) shows the resonance curves for the remaining KK gluon scenarios summarized in Table I. For comparison, the magenta line in (b) shows the result for a Z_H boson in the Littlest Higgs model with a mass of 3 TeV and $\cot\theta = 1$ (see Ref. [6]). The cuts imposed are discussed in the text.

below (above) the resonance. Since the width of KK gluons in models with a large brane kinetic term is relatively small, the resonance curves for these particles are significantly more pronounced than those for other KK gluons. For such rather narrow resonances, detector resolution effects become important. These effects are included in Figs. 1 and 2 through the smearing of particle momenta according to the ATLAS resolution.

As evident from Fig. 2, the SM non-$t\bar{t}$ background is significantly smaller in the $p_T(t \to b\ell\nu)$ distribution than in the $t\bar{t}$ invariant mass spectrum. Furthermore, the top quark transverse momentum distribution does not suffer from the ambiguity associated with the reconstruction of

the longitudinal momentum of the neutrino. On the other hand, the transverse momentum distribution only reflects information encoded in the transverse degrees of freedom.

III. NUMERICAL RESULTS

We now derive discovery limits for the KK gluon states discussed in Sec. II. We also investigate, for $M_G = 3$ TeV, how well the KK gluon states can be discriminated, and how well the couplings of these states can be measured at the LHC, and a luminosity upgraded LHC (SLHC) with a total integrated luminosity of 3000 fb^{-1}.

As the statistical tool of choice we adopt a log-likelihood test. Our expression for the log-likelihood function is

$$
\begin{aligned}
-2\log L = -2\Bigg[&\sum_i (-f_S S_i - f_B B_i \\
&+ n_{0i}\log(f_S S_i + f_B B_i) - \log(n_{0i}!)) \Bigg] \\
&+ \frac{(f_S - 1)^2}{(\Delta f_S)^2} + \frac{(f_B - 1)^2}{(\Delta f_B)^2}.
\end{aligned}
\tag{14}
$$

The sum extends over the number of bins, S_i and B_i are the number of signal and background events in the ith bin, and n_{0i} is the number of reference (eg. SM) events in the ith bin. The uncertainties on the signal and background normalizations are taken into account via two multiplicative factors, f_S and f_B, which are allowed to vary but are constrained within the relative uncertainties of the signal and background cross sections, Δf_S and Δf_B, respectively. The background consists of SM $t\bar{t}$ production, and SM non-$t\bar{t}$ background as discussed in Sec. II.

Since both the $m(t\bar{t})$ and the $p_T(t \to b\ell\nu)$ distributions have advantages and disadvantages, we use both in deriving discovery and sensitivity limits for the couplings of KK gluons. As we do not take into account common systematic uncertainties in our analysis, this procedure will lead to somewhat optimistic limits. If we use only the distribution which yields the tightest individual bounds, the results presented in this section worsen by 10%–20%.

Except for the SM $t\bar{t}$ cross section, and the backgrounds contributing to the $\ell\nu + 2$ jets final states, cross sections are only known to leading order in QCD and thus depend significantly on the renormalization and factorization scales used. In the following, we assume that QCD corrections do not significantly change the shape of the distributions analyzed in the region which contributes most to the statistical significance. Furthermore, we assume that the uncertainties for signal and background from the unknown QCD corrections are approximately equal, $f_S = f_B = f$. In this case, $\log L$ can be minimized analytically and one finds the minimum of $\log L$ to occur at

$$
f = \tfrac{1}{2}\left(1 - (\Delta f)^2 N + \sqrt{(1 - (\Delta f)^2 N)^2 + 4(\Delta f)^2 N_0}\right),
\tag{15}
$$

where

$$N = \sum_i (S_i + B_i) \tag{16}$$

is the total number of events,

$$N_0 = \sum_i n_{0i} \tag{17}$$

is the total number of reference events, and Δf is the uncertainty of the reference cross section. In the following we take $\Delta f = 0.3$. The results which we present below only minimally depend on the choice of Δf, reflecting that the normalization of the background can be obtained from the low energy part of the $m(t\bar{t})$ and $p_T(t \to b\ell\nu)$ distributions. Uncertainties from parton distribution functions, and from varying the factorization and renormalization scales are ignored in our calculation. Uncertainties from the poorly known b-tagging efficiency and light quark/ gluon jet misidentification probability are likely to be larger and difficult to quantify without actual LHC data or more accurate simulations.

A. Discovery limits

In order to derive discovery limits for the KK gluons introduced in Sec. II at the LHC we require a 5 standard deviation significance

$$-2\log L \geq 25 \tag{18}$$

from the SM prediction in the combined reconstructed $t\bar{t}$ invariant mass, and $p_T(t \to b\ell\nu)$ distribution. Results for 100 fb^{-1} and 300 fb^{-1} of data are shown in Table II. For comparison, we also list the 5σ discovery limits for a Z_H boson in the Littlest Higgs model with $\cot\theta = 1$, and for a bulk RS KK graviton, G_r, which is dominantly produced via gluon fusion [12].

To calculate the cross section for G_r production via gluon fusion in the $t\bar{t}$ channel we use the formulas of Ref. [12] with $M_4 L = 1$ and $\nu_{t,R} = 1$. Here M_4 is the Planck scale, L is the inverse of the anti-de Sitter curvature scale, and $\nu_{t,R}$ is a parameter related to the bulk mass for fermion fields. The $gg \to G_r \to t\bar{t}$ cross section scales like $(M_4 L)^{-4}$ and $(1 + 2\nu_{t,R})^2$.

The discovery limits for KK gluons in all models considered are, except for the $SO(5)$ model with $N = 1$, in the range 3.4–3.9 TeV (3.9–4.4 TeV) for 100 fb^{-1} (300 fb^{-1}). In the $SO(5)$ model with $N = 1$, the first KK excitations of the fermions are assumed to be sufficiently light so that KK gluons can decay into those. As a result, the KK gluon in this model is a very broad resonance (see Table I) which makes it considerably more difficult to detect. Our discovery limits for the basic RS case are in general agreement with those obtained in Ref. [16]. Note that KK gluons in models with a large bulk kinetic term ($\kappa r_{IR} = 5$ and $\kappa r_{IR} = 20$) couple more strongly to light quarks than top quarks and thus can be searched also for in dijet production [18]; however, no quantitative discovery limits for this channel have been derived yet. Precision electroweak data allows KK gluons with mass as low as 2–3 TeV [55]. The LHC thus should be able to significantly constrain bulk RS models.

We do not list discovery limits for an upgraded LHC with 10 times the integrated luminosity of the LHC (SLHC). Using a b-tagging efficiency of $\epsilon_b = 0.2$, which is appropriate for $t\bar{t}$ invariant masses of $\mathcal{O}(3$ TeV), we obtain 5σ limits of $M_G > 5$ TeV for KK gluons with an integrated luminosity of 3000 fb^{-1}. However, some caution is in order because a b-tagging efficiency of $\epsilon_b = 0.2$ may well be too optimistic at such huge invariant masses. Unfortunately, currently no estimates exist for ϵ_b at the SLHC in the vicinity of $m(t\bar{t}) = 5$ TeV.

The Z_H boson couples with weak coupling strength to fermions. It is therefore not surprising that the discovery limits for a Z_H boson in the $t\bar{t}$ channel are substantially weaker than those for most KK gluons. Since the Z_H boson also couples to charged leptons, the $\ell^+\ell^-$ final state is an obvious channel to search for such a particle. It should be possible to find a Z_H with mass up to 5 TeV in dilepton production at the LHC with 300 fb^{-1} [5].

The discovery limits for bulk RS KK gravitons are about a factor 3 weaker than those for KK gluons due to the strongly suppressed $G_r gg$ coupling. However, the limits listed for bulk RS KK gravitons in Table II are likely conservative. The b-tagging efficiency in the $t\bar{t}$ invariant mass range of 1–1.5 TeV is estimated to be a factor 1.5–2 higher than what we have used in our calculation [8,22].

TABLE II. Approximate 5σ discovery limits for the KK gluons introduced in Sec. II for 100 fb^{-1} and 300 fb^{-1} of data at the LHC. For comparison, we also show discovery limits for a Z_H boson in the Littlest Higgs model with $\cot\theta = 1$, and a bulk RS KK graviton with $M_4 L = 1$ and $\nu_{t,R} = 1$. See text for more details.

Model	Limit 100 fb^{-1}	Limit 300 fb^{-1}	Model	Limit 100 fb^{-1}	Limit 300 fb^{-1}
Basic RS	3.8 TeV	4.3 TeV	E_1	3.9 TeV	4.4 TeV
$\kappa r_{IR} = 5$	3.4 TeV	3.9 TeV	E_2	3.6 TeV	4.2 TeV
$\kappa r_{IR} = 20$	3.5 TeV	4.1 TeV	E_3	3.8 TeV	4.2 TeV
$SO(5),\ N = 0$	3.4 TeV	4.0 TeV	E_4	3.4 TeV	4.2 TeV
$SO(5),\ N = 1$	2.4 TeV	3.0 TeV	Z_H	2.6 TeV	2.8 TeV
KK graviton	1.3 TeV	1.4 TeV			

This will increase the 5σ discovery limits for bulk RS KK gravitons by approximately 100–200 GeV. For $\nu_{t,R} < 1$, the ZZ [56] and WW [57] channels may offer better chances to discover bulk RS KK gravitons.

In Ref. [12] G_r discovery limits were derived as a function of the top quark detection efficiency, without taking into account the non-$t\bar{t}$ background. Our calculation attempts to provide a more quantitative estimate, taking into account the non-$t\bar{t}$ background, and the reduced b-tagging efficiency at large invariant masses.

B. Discriminating KK gluon models

Once a resonance in the $t\bar{t}$ channel has been discovered, it becomes important to determine its properties in order to pin down the underlying new physics. The spin of the new particle can be determined by measuring the angular distribution of the top quarks: a scalar particle leads to an isotropic distribution, a vector boson to a distribution which is proportional to $(1 + \cos^2\theta)$, whereas the angular distribution for spin 2 particle will have a $(1 - \cos^4\theta)$ dependence [12,58]. Here, θ is the scattering angle of the top quark. Important clues can also be obtained from other final states in which the same resonance has been observed.

For the following discussion we assume that a spin 1 resonance has been found in the $t\bar{t}$ channel, however, it has not been observed elsewhere. In such a situation, KK gluons in bulk RS models become natural candidates for the state observed and it becomes interesting whether a measurement of the resonance curve in the $m(t\bar{t})$ and the $p_T(t \to b\ell\nu)$ distribution will be able to discriminate between different bulk RS models.

In order to address this question, we pursue two approaches. In this section, we calculate the "discrimination matrix" for KK gluons in the nine bulk RS models we are considering. In Sec. III C, we derive 68.3% confidence level (CL) bounds for the couplings of KK gluons. For our case study, we assume a mass of $M_G = 3$ TeV for the KK gluon. This guarantees that the LHC will be able to detect such a particle with a significance of more than 5σ in all models studied here, except the $SO(5)$, $N = 1$ case.

The discrimination matrix is constructed by performing a log-likelihood test for each pair of bulk RS models, assuming that one is correct and finding the significance of the other model as a test. The results for $M_G = 3$ TeV and an integrated luminosity of 100 fb^{-1} are presented in Table III. For smaller (larger) KK gluon masses higher (lower) significances are expected.

Table III shows that the E_i models can only be distinguished at the 1.5–3σ level. However, the remaining models can be discriminated with a significance of 4–10σ. The E_i models and non-E_i models, finally, can be separated at the 2–11σ level, except for the basic RS and the E_3 model which will be very hard to discriminate through a measurement of the resonance curve for the mass and the integrated luminosity chosen. This can be easily understood. At the resonance peak, $m(t\bar{t}) = M_G$, the $q\bar{q} \to G \to t\bar{t}$ cross section is proportional to $Br(G \to q\bar{q}) \cdot Br(G \to t\bar{t})$, where $q = u$, d, s, c denotes a light quark. For a KK gluon in the basic RS and the E_3 model, the product of the two branching fractions accidentally agrees within 15%, making it very difficult to discriminate between the two models. Nevertheless, Table III demonstrates that a measurement of the resonance curve with a luminosity of 100 fb^{-1} may well be able to eliminate a number of bulk RS models. At a luminosity upgraded LHC it should be possible to measure the couplings of a KK gluon candidate rather well, and, perhaps, uniquely identify the underlying bulk RS model nature may have chosen.

C. KK gluon coupling analysis

The interactions of KK gluons in the E_i models and models with a large brane kinetic term κr_{IR} are characterized by four couplings, g^q, $g_L^b = g_L^t$, g_R^b, and g_R^t. In all other models considered here, $g_R^b = g^q$, and there are only three independent couplings. A precise measurement of the Breit-Wigner resonance curve of KK gluons should make it possible to determine at least some of the couplings of KK gluons. Since the b-quark parton densities are much smaller than those of the light quarks, $b\bar{b} \to G \to t\bar{t}$ contributes little to the KK gluon cross section, even when $g_{L,R}^b$

TABLE III. Discrimination matrix for the KK gluons introduced in Sec. II for $M_G = 3$ TeV and an integrated luminosity of 100 fb^{-1} at the LHC. The model in each column is assumed to be the correct, measured model, and is tested against the hypothesis in each row. Since the discrimination matrix is symmetric in the limit of large statistics, we only show the entries above the diagonal.

Model	Basic RS	$\kappa r_{IR} = 5$	$\kappa r_{IR} = 20$	$SO(5),\ N = 0$	$SO(5),\ N = 1$	E_1	E_2	E_3	E_4
basic RS	0.0σ	6.1σ	10.5σ	3.1σ	7.5σ	1.7σ	2.9σ	0.0σ	2.9σ
$\kappa r_{IR} = 5$		0.0σ	5.2σ	4.3σ	7.3σ	7.1σ	7.2σ	5.4σ	6.0σ
$\kappa r_{IR} = 20$			0.0σ	7.8σ	9.9σ	10.9σ	10.9σ	9.3σ	9.7σ
$SO(5),\ N = 0$				0.0σ	4.8σ	3.7σ	3.3σ	2.8σ	1.9σ
$SO(5),\ N = 1$					0.0σ	6.8σ	5.5σ	6.8σ	4.3σ
E_1						0.0σ	1.5σ	2.0σ	2.7σ
E_2							0.0σ	3.2σ	1.6σ
E_3								0.0σ	3.2σ
E_4									0.0σ

is much larger than the SM strong coupling constant (eg. in the E_2 and E_4 models). This makes it essentially impossible to directly measure $g^b_{L,R}$. However, g^q, g^t_L, and g^t_R can, in principle, be measured.

The dependence of the $t\bar{t}$ cross section on the KK gluon couplings is of Breit-Wigner form. Since the width of the KK gluons depends on the coupling constants, the dependence of the $t\bar{t}$ cross section on the KK gluon couplings is sufficiently complicated to make the numerical extraction of sensitivity bounds very CPU time consuming when all three couplings are varied simultaneously. We do not attempt such a general analysis here. Instead, in order to get a general idea of how well the couplings of a spin 1 resonance in the $t\bar{t}$ channel may be determined at the LHC, we derive sensitivity limits for the following two limiting cases which are of interest for the models discussed here, and which greatly simplify the numerical analysis.

(1) The total width of the resonance (see Eq. (1)) is dominated by one coupling. Models which fall into this category are the basic RS, E_1 and E_3 models where g^t_R dominates the width, the $SO(5)$, $N = 0$, model where g^t_L dominates, and the models with a large brane kinetic term κr_{IR} where the width is dominated by g^q. Since the contributions of the other two couplings to the total width are negligible, the cross section is approximately bilinear in these couplings. This makes it possible to analytically solve for the coefficients multiplying these couplings in each bin of the distributions which are analyzed, provided that the coupling which dominates the width is treated as a constant. These coefficients are valid for arbitrary values of those couplings which are varied, even in regions where the dependence of the total width on those couplings

can no longer be neglected. As a result, it becomes straightforward to derive one- and two-dimensional sensitivity bounds for these couplings. In order to ensure that our results remain valid for large deviations of the couplings from their predicted values, we do take into account the dependence of the width on the couplings when deriving limits. Whenever we derive bounds for those couplings which have a negligible impact on the total width of the KK gluon, we assume that the third coupling (which dominates the width) has the default value predicted by the model considered.

Naively, one may think that the cross section should be most sensitive to the coupling which dominates the total width, g_{dom}. However, this is not the case. Most of the sensitivity comes from the immediate vicinity of the resonance, $m(t\bar{t}) = M_G$. At the resonance peak, the dependence of the numerator and the denominator on g_{dom} in the square of the KK gluon amplitude approximately cancels. In addition, the interference term between the KK gluon and the SM amplitude vanishes for $m(t\bar{t}) = M_G$. As a result, the cross section is quite insensitive to the coupling which dominates the total width.

In the following, we will derive sensitivity limits for g_{dom}, assuming that the two other couplings are fixed to the values characteristic for the model under consideration.

(2) In the remaining models, each coupling, unless it grossly deviates from its predicted value, has only a small effect on the total width. In this case we follow the approach outlined above for such couplings and derive one- and two-dimensional sensitivity limits.

In the following we present 68.3% CL limits for g^q, $g^b_L = g^t_L$, and g^t_R, and $M_G = 3$ TeV. A KK gluon with a

TABLE IV.　68.3% CL limits for the couplings of a KK gluon with mass $M_G = 3$ TeV for various integrated luminosities at the LHC and SLHC. Results are show for the basic RS model, the $SO(5)$ model with $N = 0$ and $N = 1$, and two models with a large brane kinetic term κr_{IR}. Only one coupling at a time is varied. All limits are given in units of the QCD coupling constant g_s.

	Basic RS model				$SO(5)$			
$\int \mathcal{L}dt$	100 fb^{-1}	300 fb^{-1}	3000 fb^{-1}	$\int \mathcal{L}dt$		100 fb^{-1}	300 fb^{-1}	3000 fb^{-1}
$g^q = -0.2$	$^{+0.018}_{-0.014}$	$^{+0.009}_{-0.010}$	$^{+0.003}_{-0.003}$	$g^q = -0.2$	$N=0$	$^{+0.026}_{-0.018}$	$^{+0.016}_{-0.010}$	$^{+0.004}_{-0.005}$
					$N=1$	$^{+0.068}_{-0.032}$	$^{+0.036}_{-0.022}$	$^{+0.010}_{-0.010}$
$g^t_L = 1$	$^{+1.07}_{-0.50}$	$^{+0.66}_{-0.31}$	$^{+0.18}_{-0.14}$	$g^t_L = 2.76$	$N=0$	$^{+0.65}_{-0.70}$	$^{+0.42}_{-0.35}$	$^{+0.05}_{-0.04}$
					$N=1$	$^{+0.60}_{-0.52}$	$^{+0.41}_{-0.36}$	$^{+0.23}_{-0.17}$
$g^t_R = 4$	$^{+0.64}_{-0.80}$	$^{+0.21}_{-0.39}$	$^{+0.05}_{-0.04}$	$g^t_R = 0.07$	$N=0$	$^{+0.37}_{-0.34}$	$^{+0.26}_{-0.22}$	$^{+0.14}_{-0.12}$
					$N=1$	$^{+0.67}_{-0.47}$	$^{+0.51}_{-0.32}$	$^{+0.24}_{-0.16}$
	$\kappa r_{IR} = 5$				$\kappa r_{IR} = 20$			
$\int \mathcal{L}dt$	100 fb^{-1}	300 fb^{-1}	3000 fb^{-1}	$\int \mathcal{L}dt$		100 fb^{-1}	300 fb^{-1}	3000 fb^{-1}
$g^q = -0.4$	$^{+0.14}_{-0.09}$	$^{+0.10}_{-0.06}$	$^{+0.02}_{-0.03}$	$g^q = -0.8$		$^{+0.36}_{-0.15}$	$^{+0.19}_{-0.09}$	$^{+0.03}_{-0.02}$
$g^t_L = -0.2$	$^{+0.38}_{-0.11}$	$^{+0.28}_{-0.07}$	$^{+0.05}_{-0.04}$	$g^t_L = -0.6$		$^{+0.05}_{-0.06}$	$^{+0.04}_{-0.02}$	$^{+0.01}_{-0.01}$
$g^t_R = 0.6$	$^{+0.05}_{-0.07}$	$^{+0.03}_{-0.04}$	$^{+0.01}_{-0.01}$	$g^t_R = -0.2$		$^{+0.21}_{-0.14}$	$^{+0.13}_{-0.06}$	$^{+0.03}_{-0.03}$

TABLE V. 68.3% CL limits for the couplings of a KK gluon with mass $M_G = 3$ TeV for various integrated luminosities at the LHC and SLHC. Results are show for the E_i, $i = 1, \ldots, 4$ models. Only one coupling at a time is varied. All limits are given in units of the QCD coupling constant g_s. E_1 and E_2 (E_3 and E_4) KK gluons differ only in the strength of their coupling to right-handed b quarks, see Table I.

	E_1				E_2		
$\int \mathcal{L} dt$	100 fb^{-1}	300 fb^{-1}	3000 fb^{-1}	$\int \mathcal{L} dt$	100 fb^{-1}	300 fb^{-1}	3000 fb^{-1}
$g^q = -0.2$	$+0.018$ -0.012	$+0.010$ -0.008	$+0.003$ -0.003	$g^q = -0.2$	$+0.023$ -0.015	$+0.012$ -0.010	$+0.004$ -0.004
$g^t_L = 1.34$	$+0.72$ -0.44	$+0.58$ -0.32	$+0.23$ -0.14	$g^t_L = 1.34$	$+0.90$ -0.83	$+0.65$ -0.57	$+0.24$ -0.22
$g^t_R = 4.9$	$+0.90$ -0.90	$+0.53$ -0.42	$+0.22$ -0.14	$g^t_R = 4.9$	$+0.80$ -1.02	$+0.58$ -0.64	$+0.24$ -0.21
	E_3				E_4		
$\int \mathcal{L} dt$	100 fb^{-1}	300 fb^{-1}	3000 fb^{-1}	$\int \mathcal{L} dt$	100 fb^{-1}	300 fb^{-1}	3000 fb^{-1}
$g^q = -0.2$	$+0.020$ -0.014	$+0.011$ -0.008	$+0.003$ -0.003	$g^q = -0.2$	$+0.026$ -0.017	$+0.014$ -0.008	$+0.004$ -0.004
$g^t_L = 1.34$	$+0.54$ -0.64	$+0.35$ -0.38	$+0.11$ -0.12	$g^t_L = 1.34$	$+0.76$ -0.74	$+0.48$ -0.47	$+0.18$ -0.16
$g^t_R = 3.25$	$+0.66$ -0.80	$+0.37$ -0.43	$+0.12$ -0.12	$g^t_R = 3.25$	$+0.50$ -0.68	$+0.32$ -0.52	$+0.14$ -0.16

mass of 3 TeV can be discovered with a 5σ significance or better in all models considered here, except the $SO(5)$ model with $N = 1$. We derive limits for integrated luminosities of 100 fb^{-1} and 300 fb^{-1} at the LHC, and 3000 fb^{-1} at the SLHC. As before, we combine information from the $m(t\bar{t})$ and the $p_T(t \to b\ell\nu)$ distributions. For smaller (larger) KK gluon masses, more (less) stringent limits on the couplings are obtained.

Sensitivity limits for the case when only one coupling at a time is varied are presented in Tables IV and V. In all models, except those with a large brane kinetic term κr_{IR}, the coupling to light quarks can be measured with a precision of 10%–15% for 100 fb^{-1}, and to 5% or better for 3000 fb^{-1}. In models with a large brane kinetic term κr_{IR}, decays into light quarks dominate the width (see Table I), and g^q can only be determined with an accuracy of 35%–
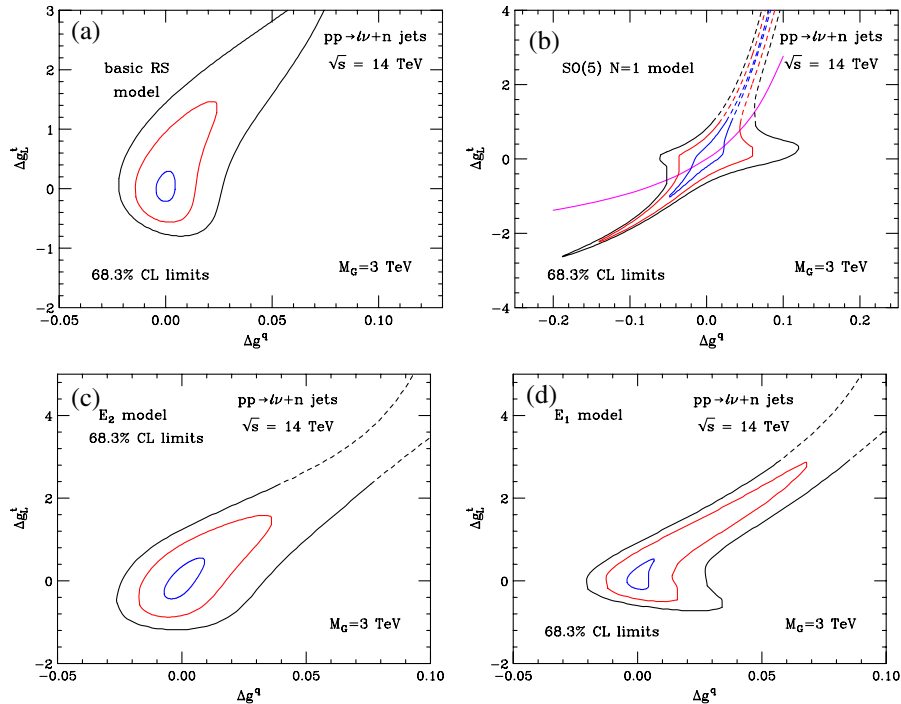
FIG. 3 (color online). Projected 68.3% CL bounds on the couplings of KK gluons with $M_G = 3$ TeV to light quarks, g^q, and left-handed top quarks, g^t_L, in (a) the basic RS, (b) the $SO(5)$ with $N = 1$, (c) the E_2, and (d) the E_1 model at the LHC with an integrated luminosity of 100 fb^{-1} (black lines) (outermost curves), 300 fb^{-1} (red lines), and 3000 fb^{-1} (blue lines) (innermost curves). The coupling of the KK gluon to right-handed top quarks is assumed to have the default value of the model considered (see Table I). The bounds are obtained from a log-likelihood analysis which combines information from the $m(t\bar{t})$ and $p_T(t \to b\ell\nu)$ distributions. Δg^q and Δg^t_L are the deviations from the default values of the coupling constants predicted by the model considered. The magenta line in part (b) indicates those couplings for which the product $g^q g^t_L$ is equal to the value predicted for the $SO(5)$ model with $N = 1$.

45% (4%–8%) for 100 fb^{-1} (3000 fb^{-1}). Note that, in addition to the allowed range for g^q listed in Tables IV and V, an interval around $g^q = 0$ cannot be excluded.

Similarly, the coupling to left-handed top quarks can be measured with a precision of 10%–100% (2%–20%) for 100 fb^{-1} (3000 fb^{-1}) except in the model with $\kappa r_{IR} = 5$ where more than 300 fb^{-1} are needed in order to rule out a vanishing of g_L^t. Similar accuracies are achievable for g_R^t, except in the $SO(5)$ model where g_R^t almost vanishes and it will be impossible to establish a nonvanishing coupling of the KK gluons to right-handed top quarks even at the SLHC.

The bounds on $g_{L,R}^t$ are in many cases significantly weaker than those for g^q. In many of the models considered here, $g_L^t \ll g_R^t$ with g_R^t being the coupling which dominates the width, or $g_R^t \ll g_L^t$, and g_L^t dominates the KK gluon width. Since the differential cross section contains terms proportional to $g_L^{t2} + g_R^{t2}$ and $g_L^t + g_R^t$, it is obvious that the sensitivity to $g_{L,R}^t$ is significantly reduced in such models.

By varying only one coupling at a time, we ignore correlations between different couplings. These correlations are expected to be particularly pronounced between g^q and $g_{L,R}^t$. This is easy to understand: the shape of the resonance curve may not change appreciably if the magnitude of g^q decreases, and that of the top quark coupling increases by a corresponding amount. Examples of two-dimensional sensitivity limits in the $g^q - g_L^t$ plane are shown in Fig. 3 for $M_G = 3$ TeV.

As expected, strong correlations are observed between g^q and g_L^t. In some cases, the limits weaken so much when both couplings are varied simultaneously that Γ_G/M_G becomes of $\mathcal{O}(1)$, and one has to worry about S-matrix unitarity being violated. In this region, the bounds on g^q and g_L^t, of course, become unreliable. The region in which $\Gamma_G/M_G > 0.5$ is indicated by dashed lines in Fig. 3. Note that the correlations between the couplings become progressively smaller with increasing integrated luminosity.

The results shown for the $SO(5)$ model with $N = 1$ deserve further discussion. Figure 3(b) shows that it will be impossible to place an upper bound on g_L^t. Even with 3000 fb^{-1}, a very narrow funnel remains where it is not possible to distinguish g_L^t and g^q from the $SO(5)$ model with $N = 1$. However, much of that funnel lies in the region where possible unitarity violations cast doubt on the reliability of our results. The peculiar shape of the contour limits in the $SO(5)$ model with $N = 1$ can be easily understood by recalling that the coupling of the KK gluon to right-handed top quarks almost vanishes in this model (see Table I). In the limit where $g_R^t = 0$ and Γ_G does not change appreciably when g^q and g_L^t are varied, the Breit-Wigner resonance curve does not change as long as the product $g^q g_L^t$ remains invariant. The line of constant $g^q g_L^t$ is indicated by the magenta line in Fig. 3(b). In practice, the small but nonzero value of $g_R^t = 0.07$, and the variation of

Γ_G are responsible for the deviation of the allowed coupling parameters from the line of constant $g^q g_L^t$. The extremely strong correlations between g^q and g_L^t make it very difficult to pin down these couplings in the $SO(5)$ model with $N = 1$. Correlations between g^q and g_R^t and g_L^t and g_R^t, however, are small in this model.

In Fig. 4 we compare the limits which can be achieved for g^q and g_L^t with 100 fb^{-1} in the E_1 and E_2 models, and the E_2 and E_4 models, respectively. KK gluons in the E_1 and E_2 models differ only by their coupling to the right-handed b quarks, and the total width. Similarly, in the E_2
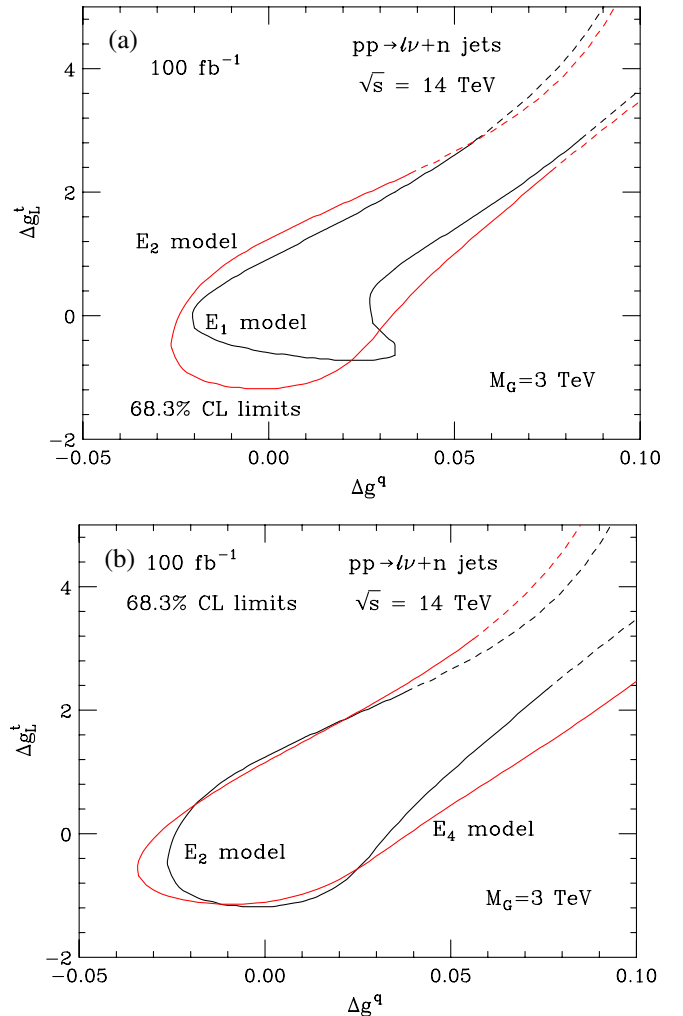
FIG. 4 (color online). Projected 68.3% CL bounds at the LHC on the couplings of KK gluons to light quarks, g^q, and left-handed top quarks, g_L^t, in (a) the E_1 and E_2 models and (b) the E_2 and E_4 models. Results are shown for $M_G = 3$ TeV and 100 fb^{-1}. The coupling of the KK gluon to right-handed top quarks is assumed to have the default value of the respective model (see Table I). The bounds are obtained from a log-likelihood analysis which combines information from the $m(t\bar{t})$ and $p_T(t \to b\ell\nu)$ distributions. Δg^q and Δg_L^t are the deviations from the default values of the coupling constants predicted by the model considered.
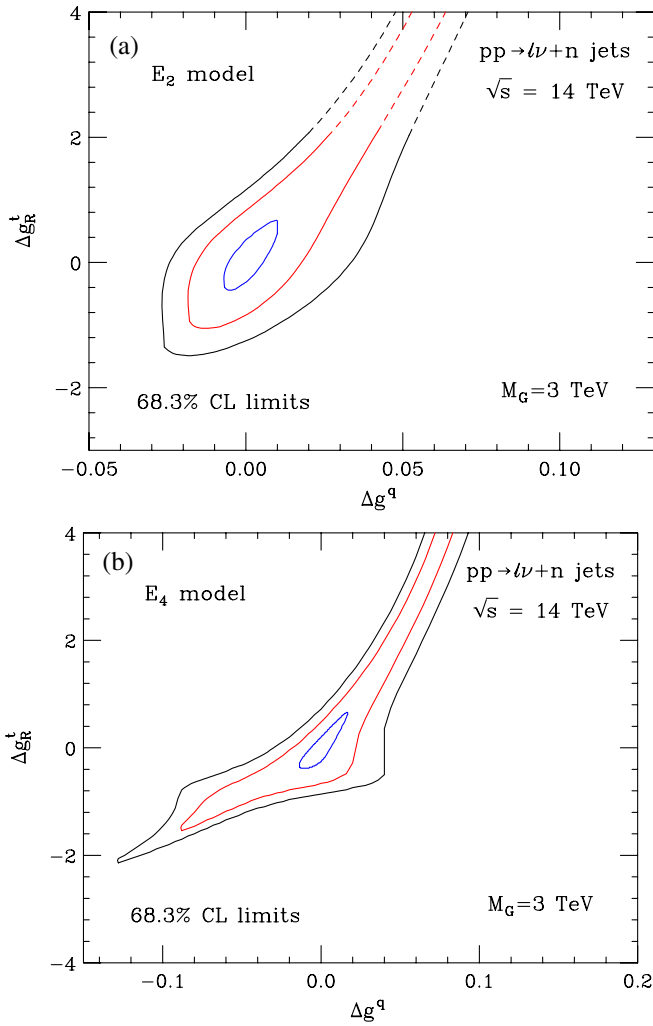
FIG. 5 (color online). Projected 68.3% CL bounds at the LHC on the couplings of KK gluons to light quarks, g^q and right-handed top quarks, g^t_R, in (a) the E_2 and (b) the E_4 model, with an integrated luminosity of 100 fb^{-1} (black lines) (outermost curves), 300 fb^{-1} (red lines), and 3000 fb^{-1} (blue lines) (innermost curves). The coupling of the KK gluon to left-handed top quarks is assumed to have the default value of the model considered (see Table I). The bounds are obtained from a log-likelihood analysis which combines information from the $m(t\bar{t})$ and $p_T(t \rightarrow b\ell\nu)$ distributions. Δg^q and Δg^t_R are the deviations from the default values of the coupling constants predicted by the model considered.

FIG. 6 (color online). Projected 68.3% CL bounds at the LHC on the couplings of KK gluons to left- and right-handed top quarks, g^t_L and g^t_R in two models with a large brane kinetic term κr_{IR}. Results are shown for 100 fb^{-1} (black lines) (outermost curves), 300 fb^{-1} (red lines), and 3000 fb^{-1} (blue lines) (innermost curves). The mass of the KK gluon is fixed to $M_G = 3$ TeV. The coupling of the KK gluon to light quarks is assumed to have the default value of the model considered (see Table I). The bounds are obtained from a log-likelihood analysis which combines information from the $m(t\bar{t})$ and $p_T(t \rightarrow b\ell\nu)$ distributions. Δg^t_L and Δg^t_R are the deviations from the default values of the coupling constants predicted by the model considered.

and E_4 models, only the coupling of the KK gluons to right-handed top quarks and the total width differ. Figure 4 demonstrates that the sensitivity limits for g^q and g^t_L in the E_i models depend only modestly on other coupling parameters. Qualitatively similar results are obtained for 300 fb^{-1} and 3000 fb^{-1}.

Strong correlations may also occur between g^q and g^t_R. As an example, we show the two-dimensional 68.3% CL sensitivity limits in the $g^q - g^t_R$ plane for the E_2 and E_4 models and $M_G = 3$ TeV in Fig. 5. In order to pin down g^t_R

with a precision of $\mathcal{O}(10\%)$ in these models, a luminosity upgrade of the LHC is needed. Similar correlations are observed between g^q and g^t_L in the two models (see Fig. 4). On the other hand, g^t_L and g^t_R display little correlation.

However, strong correlations between couplings are not only observed between g^q and $g^t_{L,R}$, but also between the couplings of KK gluons to left- and right-handed top quarks. Figure 6 shows 68.3% CL limits for g^t_L and g^t_R in two models with a large brane kinetic term κr_{IR}.

Figures 3–6 demonstrate that one-dimensional limits on the couplings of KK gluons may be totally misleading.

Although the correlations between couplings become progressively smaller with increasing integrated luminosity, they may still significantly weaken sensitivity limits at the SLHC, in some cases by up to a factor 3. Although we have not studied the correlations for cases where one of the couplings dominates the KK gluon width, we expect that strong correlations may also occur there. While it will only be possible to obtain a limited amount of information on the couplings of KK gluons at the LHC with 300 fb^{-1} or less of data when correlations are included, it will be possible to measure them with a precision of 5%–50% at the SLHC.

IV. DISCUSSION AND CONCLUSIONS

Many new physics models predict the existence of new particles decaying into a $t\bar{t}$ pair with masses in the TeV region. They lead to a peak in the $t\bar{t}$ invariant mass distribution and a Jacobian peak in the $p_T(t)$ differential cross section. In this paper we specifically studied the production of KK gluons in bulk RS models in the $t\bar{t}$ channel at the LHC. Since the couplings of KK gluons to light quarks is suppressed in many bulk RS models, the $t\bar{t}$ final state becomes their main discovery channel. The lepton + jets final state offers a good opportunity to search for such particles.

The search for resonances in the $t\bar{t}$ channel with masses in the TeV region requires the reconstruction of very energetic top quarks which faces two major difficulties. First, very energetic top quarks are strongly boosted, and their decay products are highly collimated. This leads to overlapping and merging jets from hadronically decaying top quarks. Second, the tagging efficiency for b quarks in $t\bar{t}$ events with very energetic top quarks may be up to a factor 3 smaller, and the misidentification probability of light quark or gluon jets may be up to a factor of 3 higher, than at low energies. This reduces the number of $t\bar{t}$ events which can be identified, and increases the background.

As we have shown in Ref. [33], these problems can be partially overcome by considering the $\ell\nu + n$ jets final states with one or two tagged b quarks and $n = 2, 3, 4$ instead of the canonical $\ell\nu + 4$ jets final state with two b tags, and by imposing suitable invariant mass and cluster transverse mass cuts. Using the results of Ref. [33], we calculated 5σ discovery limits for KK gluons in nine different bulk RS models by combining information from the $t\bar{t}$ invariant mass, and the $p_T(t \to b\ell\nu)$ distribution. Although information on the longitudinal degree of freedom is lost in the $p_T(t \to b\ell\nu)$ distribution, it has the advantage of a substantially smaller SM non-$t\bar{t}$ background. Our calculation takes into account the typical momentum resolution of an LHC experiment, particle identification efficiencies, and the energy loss due to b-quark decay.

Assuming a b-tagging efficiency of $\epsilon_b = 0.2$ and a light quark/gluon jet misidentification probability of $P_{j\to b} = $

1/30, as suggested by preliminary ATLAS simulations [31,32], we found that, in most models considered, KK gluons with a mass of up to 3.5–4 TeV (4–4.5 TeV) can be discovered at the LHC with an integrated luminosity of 100 fb^{-1} (300 fb^{-1}). For comparison, electroweak precision measurements require KK gluons in bulk RS models to be heavier than 2–3 TeV [55]. The LHC should therefore be able to considerably constrain such models.

For comparison, we also listed the discovery limits for the Z_H boson in the Littlest Higgs model and the KK graviton in bulk RS models in the $t\bar{t}$ channel. The discovery limits for the Z_H boson are about a factor 1.5, and those for the KK graviton are more than a factor 2, weaker than those for KK gluons. In both cases, other final states may offer a better chance to search for these particles: the Z_H boson can be discovered in Drell-Yan production with masses up to 5 TeV, whereas a KK graviton in bulk RS models can be found in the WW final state with masses up to 3.5 TeV.

We also investigated, for the example of a KK gluon with mass $M_G = 3$ TeV, how well different bulk RS models can be distinguished through a measurement of the KK gluon resonance curve. We found that, for 100 fb^{-1}, the E_i models can only be distinguished at the 1.5–3σ level. However, the remaining models can be discriminated with a significance of 4–10σ. The E_i models and non-E_i models, finally, can be separated at the 2–11σ level, except for the basic RS and the E_3 model which will be very hard to discriminate from a measurement of the KK gluon resonance curve. The conclusion to draw from this investigation is that the Breit-Wigner resonance curve in the $t\bar{t}$ final state does have some analyzing power, and thus may be helpful in discriminating new physics models.

Finally, we studied how well the KK gluon couplings can be measured at the LHC and SLHC. In the E_i, $i = 1, \ldots, 4$ models, the coupling to the right-handed b quark is an independent parameter. Since b-quark fusion contributes only little to the KK gluon cross section, it will be impossible to determine the $Gb_R b_R$ coupling from the shape of the KK gluon resonance curve in the $t\bar{t}$ final state. The remaining three couplings, g^q, $g_L^b = g_L^t$, and g_R^t, however, can be constrained from an analysis of the $m(t\bar{t})$ and $p_T(t \to b\ell\nu)$ distributions. We presented one- and two-dimensional 68.3% CL limits for these couplings. In several models, one coupling completely dominates the KK gluon width. Since interference effects vanish, and the dependence on the coupling which dominates the width approximately cancels, at the peak position of the Breit-Wigner resonance where most KK gluon events are concentrated, it will be difficult to precisely measure this coupling. We also found that correlations between couplings may strongly affect the sensitivity bounds which can be achieved. Nevertheless, at the SLHC, it should be possible to determine the couplings of a KK gluon resonance with a mass of up to 3 TeV with a precision of 5%–50% in most models.

Our results are subject to a number of uncertainties and thus should be interpreted with care. Foremost, since most background processes are not known at next-to-leading order, all our signal and background calculations have been carried out at LO, and thus are subject to substantial renormalization and factorization uncertainties. A perhaps even larger uncertainty originates from the b-tagging efficiency and the light quark and gluon jet misidentification probability at large $t\bar{t}$ invariant masses, which is only poorly known at present. PDF uncertainties, on the other hand, appear to be relatively small [59].

The numerical results presented here were obtained by combining information from the $m(t\bar{t})$ and the $p_T(t \to b\ell\nu)$ distributions. Since we ignore correlated systematic uncertainties, our results are somewhat optimistic. On the other hand, our background estimate has been deliberately conservative. Furthermore, in future studies one may in-clude additional distributions in the analysis such as the transverse momentum distribution of the charged lepton which is sensitive to the chirality of the coupling of the KK gluon to the top quark. This could potentially improve the accuracy on the KK gluon couplings which may be obtained at the LHC and SLHC.

ACKNOWLEDGMENTS

[1] M. Beneke *et al.*, arXiv:hep-ph/0003033.

[2] C. T. Hill, Phys. Lett. B **266**, 419 (1991); **345**, 483 (1995); C. T. Hill and S. J. Parke, Phys. Rev. D **49**, 4454 (1994); R. M. Harris, C. T. Hill, and S. J. Parke, arXiv: hep-ph/9911288; B. A. Dobrescu and C. T. Hill, Phys. Rev. Lett. **81**, 2634 (1998); R. S. Chivukula, B. A. Dobrescu, H. Georgi, and C. T. Hill, Phys. Rev. D **59**, 075003 (1999).

[3] For a review, see, C. T. Hill and E. H. Simmons, Phys. Rep. **381**, 235 (2003); **390**, 553(E) (2004).

[4] N. Arkani-Hamed, A. G. Cohen, and H. Georgi, Phys. Lett. B **513**, 232 (2001); N. Arkani-Hamed, A. G. Cohen, T. Gregoire, and J. G. Wacker, J. High Energy Phys. 08 (2002) 020; N. Arkani-Hamed, A. G. Cohen, E. Katz, A. E. Nelson, T. Gregoire, and J. G. Wacker, J. High Energy Phys. 08 (2002) 021; N. Arkani-Hamed, A. G. Cohen, E. Katz, and A. E. Nelson, J. High Energy Phys. 07 (2002) 034; I. Low, W. Skiba, and D. Smith, Phys. Rev. D **66**, 072001 (2002).

[5] G. Azuelos *et al.*, Eur. Phys. J. C **39S2**, 13 (2005).

[6] T. Han, H. E. Logan, B. McElrath, and L. T. Wang, Phys. Rev. D **67**, 095004 (2003); See also, J. Boersma, Phys. Rev. D **74**, 115008 (2006); J. Boersma and A. Whitbeck, Phys. Rev. D **77**, 055012 (2008).

[7] For a review, see, M. Schmaltz and D. Tucker-Smith, Annu. Rev. Nucl. Part. Sci. **55**, 229 (2005).

[8] S. González de la Hoz, L. March, and E. Ros, Report No. ATL-PHYS-PUB-2006-003, 2006.

[9] N. Arkani-Hamed, S. Dimopoulos, and G. R. Dvali, Phys. Lett. B **429**, 263 (1998).

[10] L. Randall and R. Sundrum, Phys. Rev. Lett. **83**, 3370 (1999).

[11] I. Antoniadis, Phys. Lett. B **246**, 377 (1990); J. D. Lykken, Phys. Rev. D **54**, R3693 (1996); I. Antoniadis and M. Quiros, Phys. Lett. B **392**, 61 (1997).

[12] A. L. Fitzpatrick, J. Kaplan, L. Randall, and L. T. Wang, J. High Energy Phys. 09 (2007) 013.

[13] M. Arai, N. Okada, K. Smolek, and V. Simak, Phys. Rev. D **70**, 115015 (2004); **75**, 095008 (2007).

[14] C. D. McMullen and S. Nandi, arXiv:hep-ph/0110275.

[15] K. Agashe *et al.*, Phys. Rev. D **76**, 115015 (2007).

[16] K. Agashe, A. Delgado, M. J. May, and R. Sundrum, J. High Energy Phys. 08 (2003) 050; K. Agashe, A. Belyaev, T. Krupovnickas, G. Perez, and J. Virzi, Phys. Rev. D **77**, 015003 (2008).

[17] B. Lillie, L. Randall, and L. T. Wang, J. High Energy Phys. 09 (2007) 074.

[18] B. Lillie, J. Shu, and T. Tait, Phys. Rev. D **76**, 115016 (2007).

[19] A. Djouadi, G. Moreau, and R. K. Singh, Nucl. Phys. **B797**, 1 (2008).

[20] R. Ghavri, C. D. McMullen, and S. Nandi, Phys. Rev. D **74**, 015012 (2006).

[21] D. A. Dicus, C. D. McMullen, and S. Nandi, Phys. Rev. D **65**, 076007 (2002).

[22] L. March, E. Ros, and B. Salvachúa, Report No. ATLAS-PHYS-PUB-2006-002, 2006.

[23] G. Burdman, B. A. Dobrescu, and E. Ponton, Phys. Rev. D **74**, 075008 (2006).

[24] A. S. Belyaev, I. L. Shapiro, and M. A. B. do Vale, Phys. Rev. D **75**, 034014 (2007).

[25] E. Eichten and K. D. Lane, Phys. Lett. B **327**, 129 (1994); **352**, 382 (1995).

[26] E. Cogneras and D. Pallin, Report No. ATL-PHYS-PUB-2006-033, 2006.

[27] P. H. Frampton and S. L. Glashow, Phys. Lett. B **190**, 157 (1987); Phys. Rev. Lett. **58**, 2168 (1987); M. A. Doncheski and R. W. Robinett, Phys. Lett. B **412**, 91 (1997).

[28] E. H. Simmons, Phys. Rev. D **55**, 1678 (1997).

[29] D. Choudhury, R. M. Godbole, R. K. Singh, and K. Wagh, Phys. Lett. B **657**, 69 (2007).

[30] R. Frederix and F. Maltoni, arXiv:0712.2355.

[31] A. Airapetian *et al.* (ATLAS Collaboration), Report No. CERN/LHCC/99-15, 1999.

[32] G. L. Bayatian *et al.* (CMS Collaboration), J. Phys. G **34**, 995 (2007).

[33] U. Baur and L. H. Orr, Phys. Rev. D **76**, 094012 (2007).

[34] L. Randall and M. D. Schwartz, J. High Energy Phys. 11 (2001) 003; K. Agashe, A. Delgado, and R. Sundrum, Ann. Phys. (N.Y.) **304**, 145 (2003); M. S. Carena, A. Delgado, E. Ponton, T. M. P. Tait, and C. E. M. Wagner, Phys. Rev. D **68**, 035010 (2003); K. Agashe, R. Contino, and R. Sundrum, Phys. Rev. Lett. **95**, 171804 (2005).

[35] S. J. Huber and Q. Shafi, Phys. Lett. B **498**, 256 (2001).

[36] K. Agashe and G. Servant, Phys. Rev. Lett. **93**, 231805 (2004); K. Agashe and G. Servant, J. Cosmol. Astropart. Phys. 02 (2005) 002.

[37] H. Davoudiasl, J. L. Hewett, and T. G. Rizzo, Phys. Rev. D **68**, 045002 (2003); M. S. Carena, E. Ponton, T. M. P. Tait, and C. E. M. Wagner, Phys. Rev. D **67**, 096006 (2003); M. S. Carena, A. Delgado, E. Ponton, T. M. P. Tait, and C. E. M. Wagner, Phys. Rev. D **71**, 015010 (2005).

[38] K. Agashe, R. Contino, L. Da Rold, and A. Pomarol, Phys. Lett. B **641**, 62 (2006).

[39] A. Djouadi, G. Moreau, and F. Richard, Nucl. Phys. **B773**, 43 (2007).

[40] R. Contino, L. Da Rold, and A. Pomarol, Phys. Rev. D **75**, 055014 (2007).

[41] M. S. Carena, E. Ponton, J. Santiago, and C. E. M. Wagner, Phys. Rev. D **76**, 035006 (2007).

[42] J. Pumplin, D. R. Stump, J. Huston, H. L. Lai, P. Nadolsky, and W. K. Tung, J. High Energy Phys. 07 (2002) 012.

[43] CDF and D0 Collaborations, arXiv:hep-ex/0703034.

[44] M. L. Mangano, M. Moretti, F. Piccinini, R. Pittau, and A. D. Polosa, J. High Energy Phys. 07 (2003) 001.

[45] R. Kleiss and W. J. Stirling, Z. Phys. C **40**, 419 (1988).

[46] V. Barger, T. Han, and D. G. E. Walker, Phys. Rev. Lett. **100**, 031801 (2008).

[47] A. A. Affolder *et al.* (CDF Collaboration), Phys. Rev. Lett. **87**, 102001 (2001).

[48] F. Maltoni and T. Stelzer, J. High Energy Phys. 02 (2003) 027; J. Alwall *et al.*, J. High Energy Phys. 09 (2007) 028.

[49] F. Hubaut, E. Monnier, P. Pralavorio, K. Smolek, and V. Simak, Eur. Phys. J. C **44S2**, 13 (2005).

[50] T. Sjostrand, S. Mrenna, and P. Skands, J. High Energy Phys. 05 (2006) 026.

[51] J. Conway, http://www.physics.ucdavis.edu/~conway/research/software/pgs/pgs4-general.htm.

[52] J. E. Huth *et al.*, in *Proceedings of Research Directions For the Decade: Snowmass 1990*, edited by E. L. Berger (World Scientific, Singapore, 1992), p. 134.

[53] S. Catani, Y. L. Dokshitzer, and B. R. Webber, Phys. Lett. B **285**, 291 (1992); S. D. Ellis and D. E. Soper, Phys. Rev. D **48**, 3160 (1993); S. Catani, Y. L. Dokshitzer, M. H. Seymour, and B. R. Webber, Nucl. Phys. **B406**, 187 (1993).

[54] G. C. Blazey *et al.*, arXiv:hep-ex/0005012; M. Albrow *et al.*, arXiv:hep-ph/0610012.

[55] M. S. Carena, E. Ponton, J. Santiago, and C. E. M. Wagner, Nucl. Phys. **B759**, 202 (2006); Phys. Rev. D **76**, 035006 (2007).

[56] K. Agashe, H. Davoudiasl, G. Perez, and A. Soni, Phys. Rev. D **76**, 036006 (2007).

[57] O. Antipin, D. Atwood, and A. Soni, arXiv:0711.3175.

[58] B. C. Allanach, K. Odagiri, M. A. Parker, and B. R. Webber, J. High Energy Phys. 09 (2000) 019.

[59] P. M. Nadolsky *et al.*, arXiv:0802.0007.